IOP Publishing Physica Scripta
Phys. Scr. 95 (2020) 035302 (13pp) https://doi.org/10.1088/1402-4896/ab4465

A comparison of the bremsstrahlung cross section in two frameworks: classical Lorentz–Abraham–Dirac dynamics and quantum field theory

Alexander R Kaufman and David C Latimer

Department of Physics, University of Puget Sound, Tacoma, WA 98416-1031, United States of America

E-mail: dlatimer@pugetsound.edu

Received 19 March 2019, revised 26 July 2019
Accepted for publication 13 September 2019
Published 6 February 2020

Abstract

In classical electromagnetic theory, the Lorentz–Abraham–Dirac (LAD) equation describes the dynamics of a charged particle, including radiation reaction. Though the LAD equation is derived from Maxwell's equations, consistent with the conservation of energy and momentum, it admits unphysical solutions for point-like charged particles. By assuming small radiative effects, Landau and Lifshitz (LL) develop an approximation of the LAD equation that has no pathological solutions. Though the LL approximation is dynamically sound, it is the LAD equation that has firm theoretical underpinning. As such, the difficulties encountered in LAD dynamics suggest, in part, that an electrodynamic treatment of point-like particles lies outside the classical domain. Herein, we compute the cross section of a charged particle scattered by an attractive Coulombic potential using classical LAD and LL dynamics. We then compare this with the analogous cross section in quantum field theory (QFT). In particular, we compute the cross section for a charged scalar particle incident upon another extremely massive charged scalar with a single photon in the final state. We include the following $\mathcal{O}(\alpha^3)$-radiative corrections: scalar-photon vertex correction, infrared photon emission, vacuum polarization, and two-photon exchange. We find that the classical and quantum frameworks do not produce similar cross sections. Relative to the elastic cross section, the classical bremsstrahlung cross section vastly overestimates the relative QFT cross section; this is, in part, due to the fact that the additional radiative corrections in QFT do not have a classical analog in either the LAD or LL framework.

Keywords: Lorentz–Abraham–Dirac equation, bremsstrahlung cross section, radiation reaction, quantum field theory

(Some figures may appear in colour only in the online journal)

Introduction

For more than a century, a self-consistent classical electromagnetic theory of a charged point particle has proved elusive. The primary sticking point is the inability to develop a physically sensible dynamical equation for the particle because of the complications that arise from a point particle's self force. Because an accelerated charge radiates, the ensuing energy loss effectively exerts a damping force on the particle's motion; thus, one phenomenon that a dynamical equation must accommodate is radiation reaction. Noting Larmor's formula for the radiated power [1], Lorentz was able to account for radiation damping in a nonrelativistic dynamical equation for a point particle [2]. Around the same time, Abraham took a different tack by developing a dynamical equation first for a uniformly charged shell with finite radius and then considering the limit of a vanishingly small radius [3]. Abraham's self force was derived from Maxwell's equations and, thus, was relativistically covariant even though it was developed in advance of the special theory of relativity.

A few decades later, Dirac was able to provide a covariant description of a particle's dynamics by applying the principles of conservation of energy and momentum through a small tube surrounding a point charge, where all fields are finite [4]. The result has come to be known as the Lorentz–Abraham–Dirac (LAD) equation. For a particle of charge e and mass m subject to external fields given by the field tensor $F^{\mu\nu}$, the LAD equation is

$$ma^{\mu} = eF^{\mu\nu}u_{\nu} + \frac{e^2}{6\pi}\left(\frac{\mathrm{d}}{\mathrm{d}\tau}a^{\mu} + a^2u^{\mu}\right), \tag{1}$$

where we work in natural units, in particular $c = 1$, and employ a metric with signature $(+,-,-,-)$. Here, τ represents proper time and is related to coordinate time via $t = \gamma\tau$ with $\gamma \coloneqq (1 - v^2)^{-\frac{1}{2}}$. For particle coordinate x^{μ}, we define the four-velocity and acceleration as $u^{\mu} \coloneqq \frac{\mathrm{d}}{\mathrm{d}\tau}x^{\mu}$ and $a^{\mu} \coloneqq \frac{\mathrm{d}}{\mathrm{d}\tau}u^{\mu}$, respectively. A more complete history of the development of the LAD equation can be found in [5].

Upon inspection, the most notable break from either regular Newtonian or relativistic dynamics is the fact that the LAD differential equation is third order in time. That is, to uniquely specify a particle's trajectory three initial data are required, as opposed to the usual two initial conditions. To highlight the pathological features of the solutions to the LAD equation, it is sufficient to consider a one-dimensional, nonrelativistic scenario [6]. In this case, the LAD equation reduces to Lorentz's original dynamical equation for a point charge

$$m\mathbf{a} = \mathbf{F} + \frac{e^2}{6\pi}\frac{\mathrm{d}}{\mathrm{d}t}\mathbf{a}. \tag{2}$$

Let us suppose that the particle is subject to a constant force F_0 for a time $0 \leqslant t \leqslant T$. Solving equation (2), the acceleration is

$$a(t) = \begin{cases} \left(A + \frac{1}{m}F_0\right)\mathrm{e}^{t/\tau}, & t \leqslant 0 \\ \frac{1}{m}F_0 + A\mathrm{e}^{t/\tau}, & 0 \leqslant t \leqslant T \\ \left(\frac{1}{m}F_0\mathrm{e}^{-T/\tau} + A\right)\mathrm{e}^{t/\tau}, & t \geqslant T \end{cases} \tag{3}$$

where we define $\tau \coloneqq \frac{e^2}{6\pi m}$ and A is to be set by initial conditions. If we suppose the particle's acceleration is initially zero, for all $t < 0$ then we require $A = -\frac{1}{m}F_0$, but this choice leads to a runaway solution for $t > T$, $a(t) = \frac{1}{m}F_0(\mathrm{e}^{-T/\tau} - 1)\mathrm{e}^{t/\tau}$. It is unphysical to imagine that a particle's acceleration would increase unchecked for all time when no force is acting on it. The runaway solution can be remedied by an alternate choice of initial condition. If we wish to have $a(t) \to 0$ as $t \to \infty$, then we must set $A = -\frac{1}{m}F_0\mathrm{e}^{-T/\tau}$. But, this leads to a problematic scenario for time $t < 0$; the acceleration here is $a(t) = \frac{1}{m}F_0(1 - \mathrm{e}^{-T/\tau})\mathrm{e}^{t/\tau}$. Despite the absence of a force, the acceleration of the particle is nonzero. This preacceleration anticipates the force's arrival on a time scale characterized by τ. This acausal behavior, while unpalatable, occurs over a short time scale for fundamental particles; for instance, for electrons, we find $\tau = 6.3 \times 10^{-24}$ s. These pathologies are not only a symptom of the nonrelativistic limit of the LAD equation. Indeed they persist for trajectories found from the fully relativistic LAD equation, aside from the fact that the particle's speed asymptotically approaches the speed of light for runaway solutions.

Shortly after Dirac's final covariant version of the LAD equation, Eliezer attempted to use the equation in a classical model of hydrogen with an infinitely massive nucleus, but an application to the simple one-dimensional radial infall problem resulted in an absurd solution [7]. The LAD equation yields an electron trajectory that initially does fall into the proton, but eventually, the electron reverses course, as if repelled by the proton, in a runaway solution. This behavior is not confined to the Coulomb potential. In fact, trajectories for both the attractive and repulsive 1-d central potentials can exhibit similar 'opposite' acceleration (opacceleration) [8]. These results are a consequence of integrating the LAD equation forward in time, using only initial data (namely, initial position, velocity, and acceleration) to specify the trajectory. To avoid runaways, one can drop the initial acceleration datum in favor of the requirement that the particle's acceleration vanish at sufficiently large times. To implement these boundary values, one must use backward-in-time integration [9]. With this technique, charged particles in repulsive trajectories exhibit sensible trajectories (without opacceleration) [10]. But this technique is not applicable to the case of a general attractive central potential because the value of the potential can be ill-defined at the scattering center; in this case, forward-in-time integration seems necessary [11]. If one is able to smear out the charge distribution of the scattering center, then 1-d scattering from the attractive potential does admit a solution because backward-in-time integration is possible [12], but this is not applicable for the interaction between two point charges.

Moving away from the radial infall problem, two-dimensional scattering trajectories of charged particles in the presence of a central potential can exhibit runaway trajectories with opacceleration if forward-in-time integration is used. But, so long as the impact parameter is not too small, both attractive and repulsive scattering potentials can result in sensible particle trajectories if one uses backward-in-time integration [9, 13, 14]. Considering an electron incident upon an attractive Coulombic potential, there is a minimum (nonzero) impact parameter that results in what Huschilt and Baylis term classical electron capture; that is, at this impact parameter, the scattered particle's final kinetic energy tends to zero because any initial kinetic energy has been lost due to radiation. In labeling as 'sensible' the particle trajectories derived from backward-in-time integration, we merely mean that the solutions do not exhibit runaway or opacceleration behavior. However, the lesson above still holds: eliminating runaway solutions requires solutions with preacceleration. That is, in using backward-in-time integration, the acceleration of a particle at some time is actually consistent with the force applied at some later time, though the time scale associated with this acausality is, again, small.

Given these deficiencies in the LAD equation, there have been many attempts to develop alternate dynamical equations for point particles by reducing the order of the differential equation. A discussion of such early attempts is contained in [5]. One such formulation developed by Landau and Lifshitz

(LL) has gained popularity because it approximates the Lorentz equation, (2), while sidestepping the problems of acausal and runaway solutions [15, 16]. The LL equation assumes that radiative effects are small, and thus changes in acceleration can be attributed solely to external fields. Implementing this assumption results in a physically sound dynamical equation. In the fully relativistic formulation of the LL equation, the radiation reaction term takes the same form as in the LAD equation, (1),

$$f^{\mu}_{\mathrm{LL}} = \frac{e^2}{6\pi}\left(\frac{\mathrm{d}}{\mathrm{d}\tau}a^{\mu} + a^2 u^{\mu}\right); \tag{4}$$

however, the acceleration four-vector in equation (4) is determined via the Lorentz force law

$$a^{\mu} = \frac{e}{m}F^{\mu\nu}u_{\nu}, \tag{5}$$

where $F^{\mu\nu}$ depends exclusively on fields *external* to the particle. With this assumption, the (proper) time derivative in the LL formulation, equation (4), no longer results in a dynamical equation that is third order in time

$$\frac{\mathrm{d}}{\mathrm{d}\tau}a^{\mu} = \frac{e}{m}\left(\frac{\partial F^{\mu\nu}}{\partial x^{\alpha}}u^{\alpha}u_{\nu} + F^{\mu\nu}a_{\nu}\right). \tag{6}$$

As a consequence, LL dynamics are devoid of the acausal or preaccelerative solutions encountered in LAD dynamics. Because of these nice features, the LL equation is often viewed as the correct classical description of radiation reaction. Though the LL equation is physically sound, we stress that it is, in essence, an approximation of the LAD equation.

Perhaps, a fundamental classical theory of a point-like charge is unattainable because distance scales smaller than the Compton wavelength fall within the purview of quantum mechanics. Certainly, the dynamics of extended charge distributions, like spherical shells, do not present the problems of preacceleration or runaway solutions so long as the size of the charge is greater than the classical charge radius $r_0 = e^2/(4\pi m)$ [16, 17]. For theories of extended distributions, the dynamical equations become delay differential equations. Somewhat recently, Rohrlich has developed a relativistic delay differential equation for a *finite*-sized charged particle without regard for its point-like limit [18–20]. The solutions are free of runaways and preacceleration, but some trajectories may suffer from a different pathology—post acceleration [21, 22].

If point-like charges do lie outside the classical domain, then we must turn to quantum theory for an understanding of the electrodynamics of charged particles at smaller distance scales. Regardless of whether the classical theory is attainable, there should exist a domain in which the classical and quantum theories of electrodynamics have relative agreement. Moniz and Sharp make the first attempt at bridging classical and quantum theories [23–25]. Working within the framework of nonrelativistic quantum mechanics, these authors develop a dynamical equation for the position operator of an extended charge distribution in the Heisenberg picture. Focusing on the leading order behavior, they find, in the point like limit, an expression that corresponds to the LAD equation, but their result is free from preaccelerative or runaway behavior. More recently a series of papers made connections between quantum field theory (QFT) and the LAD equation by considering the semi-classical limit (via the WKB method) of the interaction between a scalar particle and an external, accelerating potential [26–30]. These results showed that single-photon emission could effectively account for the position shift of a classical particle undergoing radiation reaction. Others have similarly shown that the change in momentum for a particle undergoing single-photon emission is consistent with that which occurs in classical radiation reaction [31]. Agreement between quantum and classical theories has also been shown in the strong-field limit [32].

Following this recent work, we wish to also compare, in this paper, the predictions of classical and quantum electrodynamics for a scattering process. Our work differs from previous groups because we are not focusing upon the radiation reaction resulting from a localized impulse, but rather upon a long-range interaction—the Coulomb interaction. In particular, we compute the differential scattering cross section for a relativistic particle of mass m and charge $-e$ that is scattered by a static Coulomb potential, consistent with a positive charge, $+e$.

In the classical framework, we use both the LAD and LL equations to determine particle trajectories. For LAD dynamics, we avoid runaway solutions by requiring the acceleration to vanish at large distances from the scattering center. Due to our choice of boundary conditions, preacceleration is present; that is, the acceleration experienced by the particle is attributable to the force experienced in the near future. Though unpalatable, preacceleration is unavoidable if we wish to exclude runaways. Rutherford scattering with radiation reaction using the LAD equation has previously been considered in [13, 14]; this work can serve as a check on our calculations. In using the LL equation, we encounter no aphysical pathologies, so the computation of particle trajectories can be formulated in the usual way as an initial value problem.

For the quantum mechanical version of our calculation, we work within the framework of QFT because the projectile particle is relativistic. The emission of bremsstrahlung radiation in electron scattering processes has been studied extensively in the literature. A survey of the outcomes is contained in [33]. In order to most closely mirror the classical scenario, we take the projectile and target particles to be scalar particles, rather than fermions. This avoids any potentially confounding effects due to magnetic dipole interactions. We assume the scattering center in the QFT case is a positively charged particle (charge $+e$) with a mass M. To mimic the static scattering potential in the classical scenario, we only consider contributions to the cross section which survive as M is taken to infinity; that is, we neglect any recoil of the scattering center. To incorporate radiation, we include a photon in the final state whose total energies range from sub-infrared values all the way up to the initial kinetic energy of the projectile. In the end, we compute the differential scattering cross section for the projectile particle, integrating over the final state photon phase space. This is comparable to the

classical differential cross section calculated using the LAD equation.

Classical cross section

We use the LAD equation, (1), to compute the classical trajectory for a particle of mass m and charge $-e$ subject to a static Coulombic potential, $V = \frac{1}{4\pi}\frac{e}{r}$. The particle has initial velocity v_i and impact parameter b_i; its initial energy is $E_i = \gamma_i m = \frac{m}{\sqrt{1-v_i^2}}$. Without loss of generality, we assume the particle's motion lies in the x–y plane. For the numerics, it is simplest to work with dimensionless coordinates. Recalling our definition of the classical electron radius, $r_0 = e^2/(4\pi m)$, we set $\bar{x} = \frac{x}{r_0}$, $\bar{y} = \frac{y}{r_0}$, and $\bar{t} = \frac{t}{r_0}$, again assuming $c = 1$. We let a dot indicate differentiation with respect to $\bar{t}$; e.g. $\dot{\bar{x}} \coloneqq \frac{\mathrm{d}\bar{x}}{\mathrm{d}\bar{t}} = \frac{\mathrm{d}x}{\mathrm{d}t}$ and $\ddot{\bar{x}} \coloneqq \frac{\mathrm{d}^2\bar{x}}{\mathrm{d}\bar{t}^2} = r_0\frac{\mathrm{d}^2x}{\mathrm{d}t^2}$. With the Coulombic scattering center, the non-dimensionalised LAD equation becomes [13]

$$\ddot{\bar{x}} = \tfrac{3}{2}\gamma^{-4}(1+\gamma^2\dot{\bar{y}}^2)\frac{\bar{x}}{\bar{r}^3} - \tfrac{3}{2}\gamma^{-2}\dot{\bar{x}}\dot{\bar{y}}\frac{\bar{y}}{\bar{r}^3} - 3\gamma^2(\dot{\bar{x}}\ddot{\bar{x}} + \dot{\bar{y}}\ddot{\bar{y}})\dot{\bar{x}} + \tfrac{3}{2}\gamma^{-1}\ddot{\bar{x}}, \tag{7}$$

$$\ddot{\bar{y}} = \tfrac{3}{2}\gamma^{-4}(1+\gamma^2\dot{\bar{x}}^2)\frac{\bar{y}}{\bar{r}^3} - \tfrac{3}{2}\gamma^{-2}\dot{\bar{x}}\dot{\bar{y}}\frac{\bar{x}}{\bar{r}^3} - 3\gamma^2(\dot{\bar{x}}\ddot{\bar{x}} + \dot{\bar{y}}\ddot{\bar{y}})\dot{\bar{y}} + \tfrac{3}{2}\gamma^{-1}\ddot{\bar{y}}, \tag{8}$$

where $\bar{r} = (\bar{x}^2+\bar{y}^2)^{\frac{1}{2}}$ and $\gamma = (1-\dot{\bar{x}}^2-\dot{\bar{y}}^2)^{-\frac{1}{2}}$.

To solve these equations, we numerically integrate backward-in-time using methods based on backward differentiation formulas from the `ODEPACK FORTRAN` library [34–36]. In backward-in-time integration, our 'intial' boundary data is, in fact, the trajectory's final position, velocity, and acceleration. In particular, we use the data

$$\bar{x}_f = 40000, \quad \dot{\bar{x}}_f = v_f, \quad \ddot{\bar{x}}_f = -\frac{\bar{x}_f}{\bar{r}_f^3} \tag{9}$$

$$\bar{y}_f = b_f, \quad \dot{\bar{y}}_f = 0, \quad \ddot{\bar{y}}_f = -\frac{\bar{y}_f}{\bar{r}_f^3}, \tag{10}$$

where v_f and b_f are the final speed and post-impact parameter. A few remarks are in order. First, we require the particle's initial energy to be $E_i = 10m$; that is, $\gamma_i = 10$ or $v_i = 0.994\,987\,437$. This energy is sufficiently relativistic to yield significant radiation, but it is not so extreme as to make likely multiple hard-photon bremsstrahlung radiation in the QFT calculation [37, 38]. To achieve the desired v_i for a trajectory, we fix the post-impact parameter b_f and then vary the final speed v_f in a binary search until backward-in-time integration yields the desired v_i to a precision of 10^{-10}. We choose the final position of the particle to be large enough that we may suppose the final acceleration is merely Coulombic; that is, this far from the scattering center, $\ddot{\bar{a}}_f$ is so small that no radiation is produced. To test dependence on $\bar{x}_f$, we increased its value by 10 000 and found its impact on the outcome was negligible (though it substantially increased computation time). Finally, we ran the computation for a sufficiently long time, $\bar{t}_i = \bar{t}_f - 2\bar{r}_f/v_f$, so that the particle's initial position is far from the scattering center resulting in $\ddot{\bar{a}}_i \sim 0$. As an additional check on our computations, we computed the energy radiated by the particle by integrating the Larmor power formula over the particle's trajectory and found that this radiated energy was equal to the change in energy of the projectile particle.

By varying the post-impact factor b_f, we are able to determine the impact parameter b_i as a function of scattering angle θ. From this, we determine the differential cross section

$$\frac{\mathrm{d}\sigma}{\mathrm{d}\Omega} = \frac{b_i}{\sin\theta}\left|\frac{\mathrm{d}b_i}{\mathrm{d}\theta}\right|. \tag{11}$$

We anticipate for small scattering angle, or large b_i, the cross section should approach the elastic limit for scattering without radiation. For larger scattering angles, the two cross sections should differ significantly. As the impact parameter decreases, the projectile particle accordingly loses more kinetic energy due to radiation. There is a minimum impact parameter at which the projectile particle loses all of its initial kinetic energy, coming to rest; this effectively results in the capture of the charged projectile. Capture occurs at some scattering angle θ_{cap} less than π. For the initial energy we consider, E_i, we find numerically the capture scattering angle to be $\theta_{\mathrm{cap}} = 79°$; this is consistent with the results of [13]. Given this behavior, the differential cross section approaches zero as θ approaches θ_{cap}.

We wish to compare the bremsstrahlung cross section to the elastic cross section in which no radiation is produced. Enforcing conservation of energy and angular momentum, relativistic dynamics yields a transcendental relationship between impact parameter and scattering angle. From these, we determine the cross section. At low energies, this reproduces the Rutherford cross section.

In figure 1, we plot in panel (a) the differential cross section for both elastic Coulombic scattering and scattering incoporating radiation reaction, as computed per the LAD equation. To highlight the differences between the two, we also include in panel (b) a plot of the ratio of the bremsstrahlung process to the elastic process. As expected, in the limit in which the scattering angle goes to zero, the bremsstrahlung cross section approaches the elastic limit. Beyond this limit, we can understand the relative differences by noting that generally, for a given impact parameter, a particle undergoing bremsstrahlung will scatter at a larger angle than that for elastic scattering. Moving away from $\theta = 0$, the bremsstrahlung cross section is actually smaller than the elastic cross section for this very reason—because the particles are scattered to larger angles. Eventually, the bremsstrahlung cross section is more than double that of the elastic process, but in the end, because scattering with radiative loss results in particle capture, the bremsstrahlung cross section drops precipitously while the elastic cross section is nonzero through full backward scattering at $\theta = \pi$.

As noted above, the LAD equation has aphysical consequences that cannot be avoided, but the LL equation has neither runaway nor preaccelerative solutions and is second order in time [15]. Given this, we also include in figure 1 a

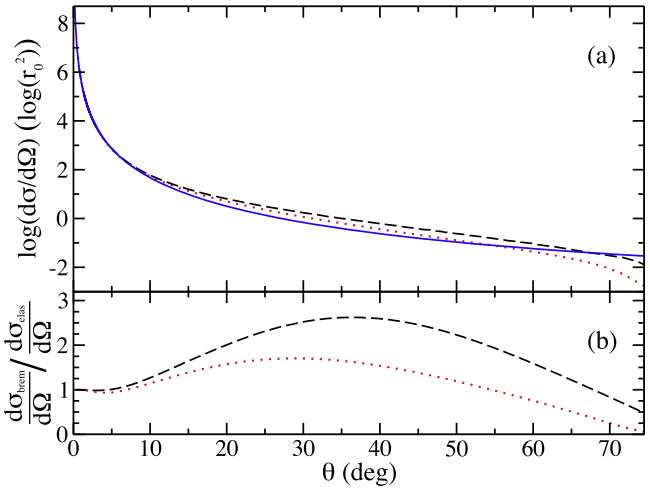

Figure 1. (a) Cross section for a charged particle scattered by an attractive Coulomb potential. The solid (blue) curve is for elastic scattering; the dashed (black) curve includes bremsstrahlung radiation, computed via the LAD equation; the dotted (red) curve includes bremsstrahlung radiation, computed via the relativistic LL equation. The cross section is expressed in units of r_0^2. (b) The ratio of the bremsstrahlung cross section relative to the elastic cross section derived from panel (a) with the dashed (black) curve computed using the LAD equation and the dotted (red) curve computed using the LL equation.

plot of the bremsstrahlung cross section computed using the relativistic LL equation. Exact analytic solutions for this problem exist in the non-relativistic limit [39], but to solve our relativistic problem, we again use the ODEPACK library to perform the numerical integration [34–36]. We use the same non-dimensionalized coordinates, $\bar{x}(\bar{t})$, $\bar{y}(\bar{t})$, developed above for the LAD equation. With the Coulombic scattering center, the non-dimensionalized LL equations become

$$\ddot{\bar{x}} = \gamma^{-1}[(1-\dot{\bar{x}}^2)\bar{F}_x - \dot{\bar{x}}\dot{\bar{y}}\bar{F}_y], \tag{12}$$

$$\ddot{\bar{y}} = \gamma^{-1}[-\dot{\bar{x}}\dot{\bar{y}}\bar{F}_x + (1-\dot{\bar{y}}^2)\bar{F}_y], \tag{13}$$

where we define

$$\bar{F}_x = -\frac{\bar{x}}{\bar{r}^3}\left[1 - \frac{2}{3}\frac{1}{\bar{r}^3}(\dot{\bar{x}}\bar{x} + \dot{\bar{y}}\bar{y})\right] - \frac{2}{3}\frac{\gamma}{\bar{r}^3}\left(\dot{\bar{x}} - 3\frac{\bar{x}^2}{\bar{r}^2}\dot{\bar{x}} - 3\frac{\bar{x}\bar{y}}{\bar{r}^2}\dot{\bar{y}}\right) - \frac{2}{3}\gamma^2\dot{\bar{x}}\left[\frac{1}{\bar{r}^4} - \frac{(\dot{\bar{x}}\bar{x} + \dot{\bar{y}}\bar{y})^2}{\bar{r}^6}\right], \tag{14}$$

$$\bar{F}_y = -\frac{\bar{y}}{\bar{r}^3}\left[1 - \frac{2}{3}\frac{1}{\bar{r}^3}(\dot{\bar{x}}\bar{x} + \dot{\bar{y}}\bar{y})\right] - \frac{2}{3}\frac{\gamma}{\bar{r}^3}\left(\dot{\bar{y}} - 3\frac{\bar{x}\bar{y}}{\bar{r}^2}\dot{\bar{x}} - 3\frac{\bar{y}^2}{\bar{r}^2}\dot{\bar{y}}\right) - \frac{2}{3}\gamma^2\dot{\bar{y}}\left[\frac{1}{\bar{r}^4} - \frac{(\dot{\bar{x}}\bar{x} + \dot{\bar{y}}\bar{y})^2}{\bar{r}^6}\right]. \tag{15}$$

We can formulate the solution of these equations as an initial value problem, integrating forward in time, with initial data

$$\bar{x}_i = -40000, \quad \dot{\bar{x}}_i = v_i, \tag{16}$$

$$\bar{y}_i = b_i, \quad \dot{\bar{y}}_i = 0, \tag{17}$$

where b_i and v_i are the initial impact parameter and speed. After evolving the particle position forward in time, we are able to numerically determine the scattering angle and then the differential scattering cross section. Referring to figure 1, the resulting cross section is qualitatively similar to that determined by LAD dynamics. Quantitatively, the cross section is enhanced by at most a factor of 1.7 relative to the elastic cross section at a scattering angle of 29°, whereas the LAD cross section is at most 2.6 times greater than the elastic cross section at a scattering angle of 35°.

Quantum cross section

We now turn to the quantum realm to compute the cross section for scattering of a charged particle via an attractive Coulombic potential with radiation. Because we consider relativistic energies, we use the framework of QFT. To best mirror the classical computation, we consider charged scalar particles to avoid confounding effects from a particle's magnetic dipole moment. Working in the rest frame of the scatterer of mass M, we take M large, neglecting recoil effects so as to approximate a static potential. In the elastic limit, this produces the Rutherford cross section at nonrelativistic energies. To model bremsstrahlung, we include one real photon in the final state.

From the outset, there are some important differences between the classical and quantum computations. Classically, the emission of radiation is a continuous process, but photon emission, in the quantum realm, is markedly discrete. In QFT, one could model a continuous process through the emission of many soft photons. Each additional photon would bring with it to the cross section a factor of the fine structure constant, $\alpha = \frac{e^2}{4\pi}$. For N final state photons, a full calculation of the cross section to order $\mathcal{O}(\alpha^{N+2})$ would be intractable. Below, we will focus upon the leading contribution to the bremsstrahlung cross section coming from one-photon emission at $\mathcal{O}(\alpha^3)$. To fully compute the cross section at this order in perturbation theory, one must not only include hard photon emission representing the bremsstrahlung radiation, but also a scalar-photon vertex correction, vacuum polarization, infrared-photon emission, and two-photon exchange with the target particle. To estimate multiple hard-photon processes, approximations must be made.

Another substantive difference between the classical and quantum formalisms is that in computing a field theoretic scattering amplitude one assumes asymptotic free states. In particular, the outgoing states are free plane waves. This can create some difficulties even for elastic scattering. At tree level, the QFT elastic cross section reproduces exactly the Rutherford cross section of classical mechanics at non-relativistic energies; however, relativistic corrections in QFT require higher order Feynman diagrams. To correctly incorporate the second Born contribution to scattering requires the use of modified propagators which encode the long range effects of the Coulomb potential [33, 40, 41]. The success of the tree-level calculation is deceptive because the phases in the modified propagators cancel, but in moving beyond this approximation, the latent issues arise.

In this work, we will focus upon single-photon emission but relegate the details of the computation to the appendix. In short, the projectile charged scalar particle interacts via the exchange of a virtual photon with the target particle emitting a real photon in the process. Because we are only interested in the final state of the projectile (and not of the emitted photon) in our computation of the cross section, we integrate over the entirety of the photon's phase space, considering all photon states with energies ranging from zero, $\omega_{\rm min} = 0$, to a maximum value set by the incoming kinetic energy of the projectile, $\omega_{\rm max} = 9\,{\rm m}$, in this case. The lower limit of the photon energy integral is problematic because the integral is logarithmically divergent, behaving as $\log(\omega_{\rm min})$ for small photon energies. This is the well-known infrared divergence problem, and it is a signal that more processes must be considered to fully compute the cross section at this order in perturbation theory [42].

To rid ourselves of the infrared divergence, we include in our computation of the cross section a radiative correction to the scalar-photon vertex. When integrating over the loop momentum in the Feynman diagram, the amplitude will diverge logarithmically if the photon is allowed to be massless. To remedy this, we give the photon a small fictitious mass μ, rendering the amplitude finite with a term dependent upon the photon mass, $\sim\log\mu$. To be consistent, we must return to the bremsstrahlung computation to give the emitted photon the same finite mass. For large photon energies, this photon mass is negligible. Given this, we introduce a small, arbitrary scale $\Lambda \gg \mu$ which defines the threshold for infrared photons. Neglecting the mass μ, the bremsstrahlung cross section is finite for photon energies between Λ and $\omega_{\rm max}$. For the infrared energies, we find that in the limit of small μ there is a logarithmic term, $\sim\log(\Lambda/\mu)$, that exactly cancels the μ-dependent logarithm from the vertex correction.

Aside from the infrared divergence that arises from the vertex correction, there is also an ultraviolet divergence for this diagram. We use dimensional regularization to compute the UV divergent diagrams and an on-shell renormalization scheme to generate the appropriate counterterms In addition to the vertex correction, we also consider the leading order correction to the vacuum polarization diagram. It too is UV divergent, and we renormalise with the on-shell scheme. Finally, the two-photon exchange diagrams are also UV divergent; again, we renormalise these with the on-shell scheme.

In figure 2(a), we plot the bremsstrahlung cross section for a projectile particle of energy 10 m. To reiterate, this cross section includes single hard photon emission, infrared emission, radiative vertex correction, vacuum polarization and elastic two-photon exchange. We note, as well, that the total cross section is well approximated by a similar calculation for fermions [43]. When we compute the contribution from infrared photon emission, we make the approximation that the photon momentum cutoff Λ is small enough that the scattering process can be considered elastic. As such, if Λ is sufficiently small the total bremsstrahlung cross section is insensitive to its particular value. In figure 2(a), we set $\Lambda = 10^{-6}\,{\rm m}$.

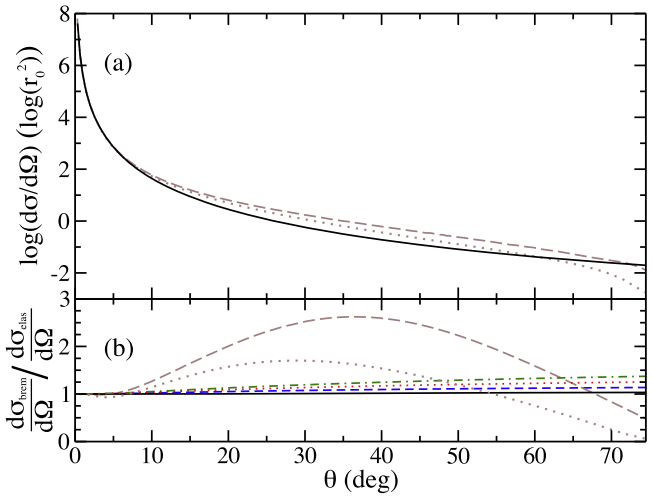

Figure 2. (a) QFT bremsstrahlung cross section for a charged particle scattered by a very massive charged particle of opposite sign. Beyond tree level, we include single (hard) photon emission, infrared photon emission, a radiative vertex correction, vacuum polarization, and two-photon exchange. The cross section is expressed in units of r_0^2. In brown, we include the classical cross sections computed using the LAD equation (dashed curve) and the Landau–Lifshitz equation (dotted curve). (b) The ratio of the bremsstrahlung cross section relative to the elastic cross section for various values of Λ. The dashed (blue) curve employs $\Lambda = 10^{-2}\,{\rm m}$; the dotted (red) curve employs $\Lambda = 10^{-4}\,{\rm m}$; the dot-dashed (green) curve employs $\Lambda = 10^{-6}\,{\rm m}$. For reference, the solid (black) curve plots the ratio of the bremsstrahlung cross section to the tree-level cross section (without the $\mathcal{O}(\alpha^3)$ elastic corrections). In brown, we include the classical ratio of cross sections computed using the LAD equation (dashed curve) and the Landau–Lifshitz equation (dotted curve).

We do not plot, in figure 2(a), the cross section resulting from the tree-level process because the bremsstrahlung and tree-level curves are nearly indistinguishable. Certainly, for small scattering angles, this should be the case, and our results confirm the two cross sections are identical for $\theta \sim 0°$. But, as we move to larger scattering angles, the bremsstrahlung cross section increases monotonically relative to the tree-level cross section, and it is roughly 3% larger than tree-level at a scattering angle of 70°. This is to be contrasted with the scattering cross section for a classical particle using LAD dynamics which differs significantly from the elastic cross section. Per figure 1(a), we find the cross section with radiation reaction is at most 2.6 times greater than the elastic cross section at a scattering angle of 35°. Another stark difference between the two frameworks is the phenomena of particle capture admitted by LAD dynamics. That is, there exists a maximum scattering angle at which the scattered particle radiates away all of its initial kinetic energy. In the QFT framework, it is certainly possible that a single photon is emitted with energy equal to the particle's initial kinetic energy. We include this possibility when we integrate over the allowed phase space for the emitted photon. But, in including all allowed final photon states, we also admit the possibility that the particle-target collision is elastic. This elastic process includes both the tree-level process and the additional radiative corrections. As a result, for *any* scattering angle, the elastic contribution to

the cross-section dominates so that scattering is possible up to and including $\theta = \pi$.

The total QFT bremsstrahlung cross section is the quantity that should be analogous to the classical cross section derived from LAD dynamics, but at the same time, the comparison could be viewed as problematic. In particular, in the QFT scenario, the *elastic* scattering cross section incorporates processes beyond tree level and, thus, beyond the analogous classical elastic cross section. Together the radiative vertex correction and infrared-photon QFT corrections lower the elastic cross section relative to tree level in a Λ-dependent manner. Specifically, the impact of these radiative corrections depends logarithmically on our choice of the artificial cutoff that we use to define what is meant by infrared photons. Experimentally, the cut off would be analogous to a detector energy resolution so that scattering would be considered elastic within some tolerance determined by Λ. Hence, elastic scattering in QFT becomes a concept dependent on the experimental design, unlike the classical scenario.

Given this, it is perhaps more sensible to compute the bremsstrahlung cross section relative to the elastic cross section. We plot this ratio in figure 2(b) for values of Λ ranging from 10^{-2} to 10^{-6} m. This quantity gives one a sense of the impact of single (hard) photon emission upon scattering without observable radiation. As we have stated, the quantity is cut-off dependent and, to a good approximation, it is given by the cross section for hard (i.e. non-infrared) single-photon emission integrated over the photon's phase space for energies from Λ to $\omega_{\max} = E - m$; that is, we have

$$\frac{\mathrm{d}\sigma_{\mathrm{brem}}}{\mathrm{d}\Omega} \Big/ \frac{\mathrm{d}\sigma_{\mathrm{elas}}}{\mathrm{d}\Omega} \approx \frac{\mathrm{d}\sigma_{\mathrm{hard}}}{\mathrm{d}\Omega}\Big|_{\omega=\Lambda}^{\omega_{\max}}. \tag{18}$$

Referring to figure 2(b), we do see that the bremsstrahlung cross section is significantly enhanced, relative to the elastic process. For $\Lambda = 10^{-6}$ m, the smallest value we consider, the cross section with hard photon emission is more than 30% greater than the elastic one around a scattering angle of 70°. But, again, this is Λ-dependent and thus not obviously relatable to the classical scenario.

Discussion

In this work, we have only considered the emission of a single hard photon as the leading approximation to a classical process that involves the continuous emission of electromagnetic radiation. In QFT, moving beyond single-photon emission involves a proliferation of diagrams to be considered. This is beyond the scope of this work; however, we did estimate the contribution to the cross section of the emission of two hard photons. We found that for a scattering angle around 70° the two-photon emission contribution to the cross section was a few percent the size of the one-photon contribution; thus, the overall effect is small. Others have developed approximate expressions for the emission of multiple photons in bremsstrahlung scattering [37, 38]. In both of these papers, the authors are primarily interested in the scattering of ultrarelativistic projectiles by a Coulomb field which allows them to neglect the impact of photon emission upon the projectile trajectories (or propagators). Reference [38] is the more refined treatment of the problem. In this paper, photon energies are divided into three categories: infrared, soft, and hard. Hard photons are those that have energies on par with the energy of the projectile particle while infrared photons are those involved involved in radiative corrections below the threshold for detection. Soft photons are in between these two classes. It is these soft photons which are assumed to have minimal impact on the particle kinematics (aside from the reduction of the particle's energy). Given this assumption, the cross section for the emission of n soft photons along with a single hard photon is computed. Relative to the tree-level cross section, each additional soft photon entails an additional factor of the fine structure constant and an energy-dependent logarithm. Though our work herein does not deal with ultrarelativistic particles, it is likely multiple photon emission modifies our cross section in a similar way. As such, it seems unlikely that including multiple photon emission in a detailed calculation will bridge the difference between the classical and QFT cross sections.

Overall, we see that the QFT and classical cross sections fail to agree, except in the no-radiation limit (i.e. $\theta \approx 0$). In order to faithfully make a comparison between the QFT and classical frameworks, we focused upon the cross section because it is a physically measurable quantity. However, in the QFT case, this involves a choice of *what* sort of cross section to compute. To mirror the classical situation, we opted to consider only the final state of the charged projectile, integrating over the allowed photon phase space. As a consequence, the bremsstrahlung cross section was independent of the arbitrary cutoff for infrared photons (assuming this cutoff is sufficiently small), but this leads to only a few percent correction of the cross section relative to tree level, in part, because radiative corrections to the elastic cross section are, overall, negative. This cut-off independent quantity should be comparable to the classical cross section, but the presence of radiative corrections to the elastic cross section move beyond the classical scenario *even* in the no-radiation regime. This suggests that it is, perhaps, more sensible to use the elastic cross section (with radiative corrections) as the baseline to compare the bremsstrahlung cross section in the QFT framework. As we have seen, this is dependent upon the artificial infrared cutoff, making a comparison to the classical result impossible. Because of these difficulties, we find the QFT and classical descriptions of bremsstrahlung scattering from a Coulomb potential incommensurable at the energy scale under consideration.

In this paper, we have opted to use the standard interaction picture to compute scattering cross sections in QFT. Because we wish the projectile particle to be scattered by a static field, we require the target projectile to be extremely massive. One advantage of this approach is that we can easily relax the assumption of the massive scatterer and consider (more realistic) recoil effects in the future. However, to solve the problem at hand, it is also possible to work in the Furry picture [44] as applied to scalar quantum electrodynamics so

that the projectile can scatter from a static background external field.

Appendix. QFT cross section

In this appendix, we discuss some of the details of the QFT calculations. First, we begin with the Lagrangian for the theory under consideration before discussing the contributions to the $\mathcal{O}(\alpha^3)$ scattering cross section.

The Lagrangian for scalar electrodynamics is

$$\mathcal{L} = (D_\mu \phi)^*(D^\mu \phi) - m^2\phi^*\phi - \frac{1}{4}F^{\mu\nu}F_{\mu\nu} - \frac{1}{4}\lambda(\phi^*\phi)^2, \tag{19}$$

where the covariant derivative is $D_\mu = \partial_\mu + iqA_\mu$ with $q = -e$ for the projectile particle and $F_{\mu\nu} = \partial_\mu A_\nu - \partial_\nu A_\mu$. The ϕ^4 term is needed to render finite higher order cross sections [45], though the interactions mediated by this term are irrelevant for our calculations at present order in perturbation theory. The target scalar particle, Φ, has an identical Lagrangian modulo the changes: $m \mapsto M$, $q \mapsto +e$, and $\lambda \mapsto \Lambda$. The two scalar particles are effectively coupled via electromagnetism, but one could also introduce a direct coupling term to the Lagrangian $\sim g\phi^*\phi\Phi^*\Phi$. For a dimensionless coupling g, this term has mass dimension four, and thus, it is a *possible* interaction that we might consider. But, we find it is in fact *necessary* to include this interaction. Below, we show that the two-photon exchange diagrams between the projectile and target particles are UV divergent. In order to render the theory finite, we must renormalise the direct coupling g; this is analogous to the need for the ϕ^4 term for a single scalar field.

A.1. Tree-level elastic scattering

We include details regarding the radiative corrections to the scattering cross section in which the scalar particle ϕ of mass m scatters off another scalar particle Φ of mass M through single photon exchange. We use FORM [46] to aid our algebraic manipulations.

We first examine the tree-level contribution, figure A1, to the amplitude. Let p and P be the incoming momenta for ϕ and Φ, respectively; outgoing momenta for these particles carry primes. The momentum transfer to ϕ is $q = p' - p = P - P'$. We will work in the rest frame of Φ so that $P = (M, \mathbf{0})$. We also assume that Φ is very massive, $M \gg m$, so that its recoil is minimal. With this assumption the energy transfer to ϕ is negligible so that the collision is elastic; that is, we assume $q^0 \approx \frac{-|\mathbf{q}|^2}{2M} \approx 0$. Keeping only leading order terms, we find the tree-level contribution to the amplitude is

$$\mathcal{M}_{\text{tree}} \approx -\frac{16\pi\alpha ME}{|\mathbf{q}|^2}, \tag{20}$$

where $p^0 = E \approx p'^0$ and $q^2 \approx -|\mathbf{q}|^2 = -2|\mathbf{p}|^2(1 - \cos\theta)$ with the scattering angle given by $\cos\theta = \hat{\mathbf{p}}' \cdot \hat{\mathbf{p}}$. The resulting cross section is

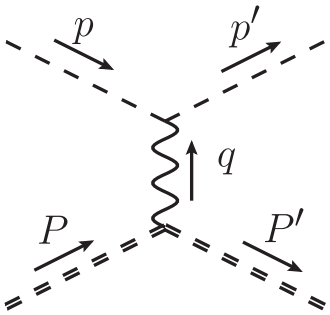

Figure A1. Tree level contribution to elastic scattering. The projectile, ϕ, is indicated by a single dashed line, and the massive scalar, Φ, is indicated by a double dashed line.

$$\frac{d\sigma_{\text{tree}}}{d\Omega} = \frac{\alpha^2 E^2}{4|\mathbf{p}|^4 \sin^4\frac{\theta}{2}}. \tag{21}$$

A.2. Hard photon emission

We now consider single photon emission that can occur when ϕ scatters. The relevant diagrams are in figure A2. Because we consider the mass of Φ to be large, $M \gg m$, photon emission from Φ is negligible, so we do not consider it. As before the incoming momenta of the scalars are p and P, and we work in the very massive scalar particle's rest frame, $P = (M, \mathbf{0})$. Also, the momentum transferred to the scalar ϕ remains $q = P - P' \approx (0, \mathbf{q})$. A transverse, real photon of momentum $k = \omega(1, \hat{\mathbf{k}})$ and polarization ϵ is in the final state; we require $k^2 = 0$ and $\epsilon \cdot k = 0$. The final momentum of the scattered scalar, ϕ, is $p'' = p + q - k$; in our approximation ($M \gg m$), the time-like component of this equation is consistent with $E'' = E - \omega$. In these limits, the amplitude simplifies to

$$\mathcal{M}_{\text{hard}} \approx 4e^3\frac{1}{q^2}\epsilon^*_\mu\left(ME\frac{p''^\mu}{p''\cdot k} - ME''\frac{p^\mu}{p\cdot k} - P^\mu\right). \tag{22}$$

In computing the cross section, we will sum over the final photon polarization states

$$\sum_\mu |\mathcal{M}_{\text{hard}}|^2 = -\frac{16e^6}{q^4}M^2\left(\frac{E^2m^2}{(p''\cdot k)^2} + \frac{E''^2m^2}{(p\cdot k)^2} + 1 - 2\frac{E''E(p''\cdot p)}{(p''\cdot k)(p\cdot k)} - 2\frac{E''E}{p''\cdot k} + 2\frac{E''E}{p\cdot k}\right). \tag{23}$$

The final state contains three particles with a total of nine momentum components subject to four constraints from energy-momentum conservation; thus, the final state has five independent degrees of freedom. In computing the differential cross section, we choose as our independent degrees of freedom the scalar particle's polar and azimuthal angles, θ and φ, along with the photon's energy ω and scattering angles θ_k and φ_k. After including appropriate phase space factors and integrating over the constrained momenta, we find the

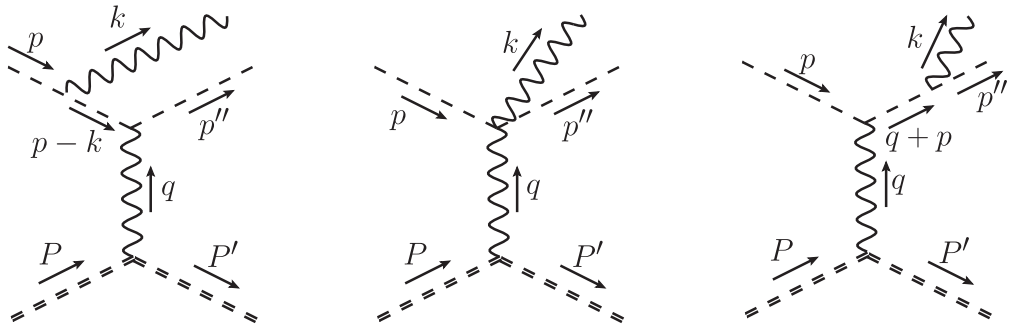

Figure A2. Feynman diagrams contributing to single hard photon emission.

differential cross section

$$\mathrm{d}\sigma_{\mathrm{hard}} = \frac{\alpha^3}{(4\pi)^2}\frac{\sum_\mu |\mathcal{M}|^2}{e^6 M^2}\frac{|\mathbf{p}''|}{|\mathbf{p}|}\omega \mathrm{d}\omega\, \mathrm{d}\Omega_k\, \mathrm{d}\Omega \tag{24}$$

with the proviso that $\mathbf{q} \equiv \mathbf{p}'' + \mathbf{k} - \mathbf{p}$ and $|\mathbf{p}''| \equiv \sqrt{|\mathbf{p}|^2 - 2E\omega + \omega^2}$.

Because we are only interested in the scattering solid angle $\mathrm{d}\Omega$ of the projectile, we numerically integrate over all photon emission angles $\mathrm{d}\Omega_k$. Finally, we wish to integrate over photon energies (or momenta, more precisely) up to the kinetic energy of the incoming projectile, $\omega_{\max} = E - m$; however, setting the lower limit of photon energy to zero is problematic because the cross section for emitting an infrared photon $\omega \sim 0$ is logarithmically divergent. We rectify this by introducing an infrared cutoff $\omega_{\min} = \Lambda$ so that the denominators in equation (23) do not vanish. The cutoff should be on par with or less than the experimental detector resolution. In a scattering experiment, if a photon is emitted with energy less than this cutoff, then the process is experimentally indistinguishable from elastic scattering. Theoretically, such a process must be considered in conjunction with other radiative corrections to the elastic tree-level scattering.

A.3. Infrared photon emission

We now describe our treatment of infrared-photon emission. In order to regulate the logarithmic dependence, we suppose the photon has a small fictitious mass μ, assumed to be much smaller than Λ. Because we now assume a massive photon, we must be more precise in the meaning of this cutoff; Λ represents the maximum *momentum* of the emitted photon so that the maximum *energy* of the emitted photon is $\omega_{\max} = \sqrt{\mu^2 + \Lambda^2}$. The emitted photon's momentum four vector, $k = (\omega, \mathbf{k})$, now satisfies $k^2 = \mu^2$ and $|\mathbf{k}| < \Lambda$.

For infrared photon emission, we consider the scattering approximately elastic, $|\mathbf{p}''| \approx |\mathbf{p}|$, or using the notation from the tree-level process, we set $\mathbf{p}'' \approx \mathbf{p}'$ and thus $E'' \approx E$. In this limit, the squared amplitude, equation (23), simplifies a bit

$$\sum_\mu |\mathcal{M}|^2 = -\frac{16e^6}{q^4}E^2M^2\left(\frac{m^2}{(p'\cdot k)^2} + \frac{m^2}{(p\cdot k)^2} - \frac{2p'\cdot p}{(p'\cdot k)(p\cdot k)} - \frac{2}{p'\cdot k} + \frac{2}{p\cdot k}\right), \tag{25}$$

keeping only the logarithmically divergent terms. To get the cross section, we supply the usual phase space factors but note that the tree-level differential cross-section can be factored out of the infrared-photon emission cross-section

$$\mathrm{d}\sigma_{\mathrm{infr}} \approx -\mathrm{d}\sigma_{\mathrm{tree}}\, e^2 \int \frac{\mathrm{d}^3k}{(2\pi)^3}\frac{1}{2\omega}\left(\frac{m^2}{(p'\cdot k)^2} + \frac{m^2}{(p\cdot k)^2} - \frac{2p'\cdot p}{(p'\cdot k)(p\cdot k)} - \frac{2}{p'\cdot k} + \frac{2}{p\cdot k}\right). \tag{26}$$

All but one of the integrals in equation (26) can be easily evaluated in spherical coordinates. First, we introduce the notation $p = E(1, \mathbf{v})$ and $p' = E(1, \mathbf{v}')$ with scattering angle defined as before $\hat{\mathbf{v}}\cdot\hat{\mathbf{v}}' = \cos\theta$. As an example, we have

$$\int \frac{\mathrm{d}^3k}{(2\pi)^3}\frac{1}{2\omega}\frac{m^2}{(p\cdot k)^2} = \frac{1}{8\pi^2}\left[\frac{1}{|\mathbf{v}|}\log\left(\frac{1-|\mathbf{v}|}{1+|\mathbf{v}|}\right) + \log\frac{4\Lambda^2}{\mu^2}\right], \tag{27}$$

to leading order in μ. Swapping p' for p in the above integral yields the same result. Similarly, the last two terms in equation (26) cancel each other.

For the remaining integral in equation (26), we use Feynman's trick to combine the two factors in the denominators [42]

$$\frac{1}{AB} = 2\int_{-1}^{1}\frac{\mathrm{d}x}{[(1+x)A + (1-x)B]^2}. \tag{28}$$

Using this identity, we can rewrite the remaining integral as

$$\int \frac{\mathrm{d}^3k}{(2\pi)^3}\frac{1}{2\omega}\frac{2p'\cdot p}{(p'\cdot k)(p\cdot k)} = \int_0^1 \mathrm{d}x \int \frac{\mathrm{d}^3k}{(2\pi)^3}\frac{1}{2\omega}\frac{p'\cdot p}{(\tilde{p}\cdot k)^2}, \tag{29}$$

where $\tilde{p} = (E, \tilde{\mathbf{p}}) \coloneqq \frac{1}{2}[p'(1+x) + p(1-x)] = p + \left(\frac{1+x}{2}\right)q$. The integral over d^3k is the same, *mutatis mutandis*, as in equation (27)

$$\int \frac{\mathrm{d}^3k}{(2\pi)^3}\frac{1}{2\omega}\frac{2p'\cdot p}{(p'\cdot k)(p\cdot k)} = \frac{p'\cdot p}{8\pi^2}\int_{-1}^{1}\mathrm{d}x\frac{1}{E^2 - |\tilde{\mathbf{p}}|^2}\left[\log\frac{4\Lambda^2}{\mu^2} + \frac{E}{|\tilde{\mathbf{p}}|}\log\left(\frac{E-|\tilde{\mathbf{p}}|}{E+|\tilde{\mathbf{p}}|}\right)\right]. \tag{30}$$

We solve the second integral in equation (30) numerically though closed form expressions do exist [47]. The integral

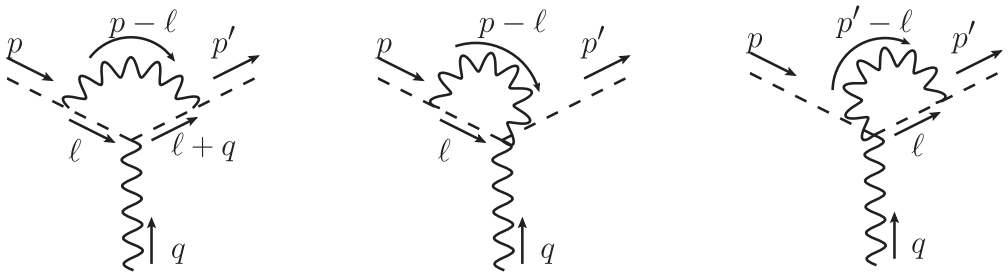

Figure A3. Diagrams contributing to the vertex correction of the light scalar, ϕ.

involving the logarithmically divergent term is easily evaluated in closed form

$$\int_{-1}^{1} \mathrm{d}x \frac{1}{E^2 - |\tilde{\mathbf{p}}|^2} = -\frac{4}{q^2}\beta \log\left(\frac{1+\beta}{1-\beta}\right), \tag{31}$$

where we define $\beta \coloneqq \sqrt{q^2/(q^2 - 4m^2)}$.

Putting all these terms together, the infrared-photon emission cross section is $\mathrm{d}\sigma_{\mathrm{infr}} = \mathrm{d}\sigma_{\mathrm{tree}}\delta_{\mathrm{infr}}$ with

$$\begin{aligned}\delta_{\mathrm{infr}} \approx \frac{\alpha}{\pi}\Bigg\{&\frac{1}{|\mathbf{v}|}\log\left(\frac{1+|\mathbf{v}|}{1-|\mathbf{v}|}\right) + \log\frac{\mu^2}{4\Lambda^2} \\ &+ \left(1 - 2\frac{m^2}{q^2}\right)\beta\log\left(\frac{1-\beta}{1+\beta}\right)\log\frac{\mu^2}{4\Lambda^2} \\ &+ \frac{1}{4}(2m^2 - q^2)\int_{-1}^{1}\mathrm{d}x\frac{1}{E^2 - |\tilde{\mathbf{p}}|^2}\frac{E}{|\tilde{\mathbf{p}}|}\log\left(\frac{E - |\tilde{\mathbf{p}}|}{E + |\tilde{\mathbf{p}}|}\right)\Bigg\}\end{aligned} \tag{32}$$

assuming small μ and Λ. We note that the cross section is logarithmically divergent as the fictitious photon mass goes to zero, and it also depends explicitly on the momentum cutoff Λ. By combining the infrared-photon emission with the radiative vertex correction, we will find an overall cross section independent of μ.

We examine the extreme cases with $-q^2 \ll m^2$ and $-q^2 \gg m^2$, keeping only the logarithmically divergent terms

$$\delta_{\mathrm{infr}} \approx \frac{\alpha}{\pi}\frac{q^2}{3m^2}\log\frac{\mu^2}{4\Lambda^2} \quad \text{(NR)}, \tag{33}$$

$$\delta_{\mathrm{infr}} \approx \frac{\alpha}{\pi}\left[1 - \log\left(-\frac{q^2}{m^2}\right)\right]\log\frac{\mu^2}{4\Lambda^2} \quad \text{(ER)}. \tag{34}$$

A.4. Vertex correction

In order to compute the scattering cross section to $\mathcal{O}(\alpha^3)$, we must include $\mathcal{O}(\alpha^2)$ correction to the tree-level elastic scattering amplitude. This involves a vertex correction along with a correction to the photon propagator. We begin with the vertex correction by introducing the form factor $F(q^2)$ so that the Feynman rule for the photon-scalar vertex is $-\mathrm{i}.e.F(q^2)(p'^{\mu} + p^{\mu})$. We compute only the $\mathcal{O}(\alpha)$ correction to the form factor $F(q^2) \approx 1 + F^{(1)}(q^2)$. The nonzero diagrams are contained in figure A3. The correction is ultraviolet divergent so we renormalise with the on-shell renormalization scheme. It is also infrared divergent, so we will introduce a fictitious photon mass μ for the loop photons which will cancel the photon mass that appeared in the infrared-photon emission process. Then vertex correction is

$$F^{(1)}(q^2) = \frac{\alpha}{4\pi}\Bigg\{(2q^2 - 4m^2)I_{\mathrm{IR}} + 2\log\frac{m^2}{\mu^2} \tag{35}$$

$$+4\left(1 - 2\frac{m^2}{q^2}\right)\beta\log\left(\frac{1+\beta}{1-\beta}\right) - 4\Bigg\}. \tag{36}$$

The integral I_{IR} is divergent in the limit of vanishing photon mass, μ,

$$I_{\mathrm{IR}} = \int_0^1 \mathrm{d}z \int_0^{1-z} \mathrm{d}y \frac{1}{(1-z)^2 m^2 - y(1-y-z)q^2 + z\mu^2}. \tag{37}$$

For small μ, one can use standard tricks [48] to get a more tractable expression which can then be evaluated in closed form

$$\begin{aligned}I_{\mathrm{IR}} &\approx \frac{1}{2}\int_0^1 \mathrm{d}\xi \frac{1}{m^2 - \xi(1-\xi)q^2}\log\left(\frac{m^2 - \xi(1-\xi)q^2}{\mu^2}\right) \\ &= -\frac{1}{q^2}\beta\log\left(\frac{1-\beta}{1+\beta}\right)\log\left(\frac{-\mu^2}{q^2}\right)\end{aligned} \tag{38}$$

$$\begin{aligned}&+ \frac{1}{2q^2}\beta\Bigg\{\log\left(\frac{1-\beta}{1+\beta}\right)\log\left(-\frac{m^2}{q^2}\left(1 - \frac{4m^2}{q^2}\right)\right) \\ &+ 2\mathrm{Li}_2\left(\frac{1}{2}(1+\beta)\right) - 2\mathrm{Li}_2\left(\frac{1}{2}(1-\beta)\right)\Bigg\},\end{aligned} \tag{39}$$

where the dilogarithm is given by

$$\mathrm{Li}_2(z) = -\int_0^z \mathrm{d}z' \frac{\log(1-z')}{z'}. \tag{40}$$

In the two limiting cases, we find the vertex correction is

$$F^{(1)}(q^2) \approx \frac{\alpha}{4\pi}\left(-1 + \frac{2}{3}\log\frac{m^2}{\mu^2}\right)\frac{q^2}{m^2} \quad \text{(NR)}, \tag{41}$$

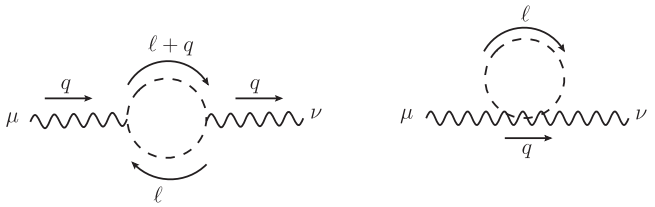

Figure A4. Leading diagrams which contribute to vacuum polarization.

$$F^{(1)}(q^2) \approx \frac{\alpha}{2\pi}\left\{\log\left(\frac{m^2}{\mu^2}\right)\left[1 - \log\left(-\frac{q^2}{m^2}\right)\right] - \frac{1}{2}\log^2\left(-\frac{q^2}{m^2}\right) + 2\log\left(-\frac{q^2}{m^2}\right) + \frac{\pi^2}{6} - 2\right\} \quad \text{(ER)}. \tag{42}$$

A.5. Vacuum polarization

The photon propagator has an $\mathcal{O}(\alpha)$ correction due to the vacuum polarization diagrams in figure A4. To this order, the propagator is given by $\frac{-ig_{\mu\nu}}{q^2}(1 + \Pi(q^2))$ with the correction evaluated in the on-shell renormalization scheme

$$\Pi(q^2) = \frac{\alpha}{\pi}\int_0^1 \mathrm{d}z(2z - 1)^2 \log\left(\frac{q^2}{m^2}(z^2 - z) + 1\right). \tag{43}$$

This integral can be evaluated in closed form, but we only include the nonrelativistic, $-q^2 \ll m^2$, and extreme relativistic, $-q^2 \gg m^2$, limits in this appendix

$$\Pi(q^2) \approx -\frac{\alpha}{30\pi}\frac{q^2}{m^2} \quad \text{(NR)}, \tag{44}$$

$$\Pi(q^2) \approx \frac{\alpha}{3\pi}\left[\log\left(-\frac{q^2}{m^2}\right) - \frac{8}{3}\right] \quad \text{(ER)}. \tag{45}$$

A.6. Two-photon exchange

To complete the $\mathcal{O}(\alpha^3)$ correction to the elastic cross section, we include the two-photon exchange diagrams in figure A5. Counting powers of loop momentum k in the integrand shows that all diagrams have logarithmic UV divergences, and this divergence persists when we sum the diagrams. Because we are working with scalar particles, there is an additional term with mass dimension four in the Lagrangian that *can* be present, directly coupling the two scalars, $\mathcal{L}_{\text{int}} \sim g\phi^*\phi\Phi^*\Phi$. Given the divergence of the diagrams in figure A5, we *must* include this term so that the renormalization of the coupling g can render finite the scattering amplitude; this is akin to the need for a ϕ^4 term in a field theory for a single scalar field [45]. This direct interaction between the scalar particles requires the introduction of new interactions beyond the classical paradigm, so we only consider the coupling g insofar as it permits us to render finite the contribution from two-photon exchange. As an aside, we note that if we were considering the electromagnetic scattering of two fermions, this UV divergence would not be present [49, 50].

To this end, we work in the static limit $M \to \infty$ and require the two-photon exchange contribution to yield the tree-level amplitude as the momentum transfer vanishes, $q^2 \to 0$. With these constraints, it is only the first two diagrams in figure A5 that contribute. In addition to the UV divergence, these two box diagrams contain IR divergences. Using a trick from [51], we can isolate the IR divergent terms

$$\begin{aligned}\frac{q^2}{[k^2 - \mu^2][(k-p)^2 - m^2][(k+P)^2 + M^2][(k+q)^2 - \mu^2]} &= \frac{1}{[k^2 - \mu^2][(k-p)^2 - m^2][(k+P)^2 + M^2]} \\ &+ \frac{1}{[(k-p)^2 - m^2][(k+P)^2 + M^2][(k+q)^2 - \mu^2]} \\ &- \frac{2k\cdot(k+q)}{k^2[(k-p)^2 - m^2][(k+P)^2 + M^2](k+q)^2}.\end{aligned} \tag{46}$$

The first two terms on the righthand side are IR divergent whereas the last term is not. These IR divergences are canceled by IR divergences from infrared photon emission. Above, we only considered infrared photon emission from the projectile particle because the analogous process for the massive target vanishes in the static limit; however, the *interference* between the infrared photon emission from the projectile and target particles has an IR divergence that cancels that from the box diagrams. The details of the infrared photon emission from scalar particles are identical to those from fermions [52]. After canceling the IR divergent terms, the remaining terms in the box contributions to the amplitude can be expressed in closed form [47]; however, we choose to numerically integrate the parameter integrals. In the end, we find, numerically, a correction to the elastic amplitude of the form $\mathcal{M}_{\text{box}} = \mathcal{M}_{\text{tree}}\delta_{\text{box}}$.

A.7. Radiative correction to elastic scattering

We now combine the radiative corrections to the tree-level elastic scattering amplitude

$$\mathcal{M}_{\text{corr}} \approx \mathcal{M}_{\text{tree}}(1 + F^{(1)}(q^2) + \Pi(q^2) + \delta_{\text{box}}(q^2)). \tag{47}$$

From this, we can compute the cross section for elastic scattering, accurate to $\mathcal{O}(\alpha^3)$, sans infrared emission

$$\begin{aligned}\mathrm{d}\sigma_{\text{corr}} \approx \mathrm{d}\sigma_{\text{tree}}(1 &+ 2\,\mathrm{Re}[F^{(1)}(q^2)] \\ &+ 2\,\mathrm{Re}[\Pi(q^2)] + 2\,\mathrm{Re}[\delta_{\text{box}}(q^2)]).\end{aligned} \tag{48}$$

This contribution to the elastic cross section should be combined (incoherently) with the infrared-photon emission cross section given the fact that infrared-photon emission is experimentally indistinguishable. Taken together, this cross section will now be rid of the infrared divergence by cancellation of the fictitious regulator μ. We show this by just focusing on the μ-dependent terms as derived from equations (32) and (36)

$$(2F^{(1)}(q^2) + \delta_{\text{infr}})_{\text{IR}} \tag{49}$$

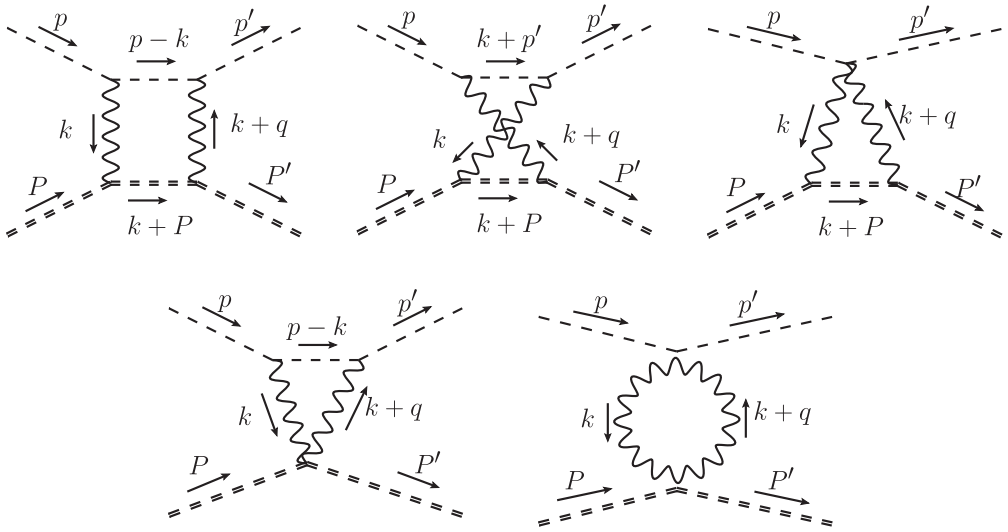

Figure A5. Two-photon exchange diagrams which contribute to the elastic scattering cross section at $\mathcal{O}(\alpha^3)$.

$$= \frac{\alpha}{\pi}\left\{\left[1 + \left(1 - 2\frac{m^2}{q^2}\right)\beta \log\left(\frac{1-\beta}{1+\beta}\right)\right]\log\frac{\mu^2}{4\Lambda^2} - \left(1 - 2\frac{m^2}{q^2}\right)\beta \log\left(\frac{1-\beta}{1+\beta}\right)\log\left(\frac{\mu^2}{-q^2}\right) + \log\frac{m^2}{\mu^2}\right\} \tag{50}$$

$$= \frac{\alpha}{\pi}\left\{\left(1 - 2\frac{m^2}{q^2}\right)\beta \log\left(\frac{1-\beta}{1+\beta}\right)\log\frac{-q^2}{4\Lambda^2} + \log\frac{m^2}{4\Lambda^2}\right\}. \tag{51}$$

Indeed, any dependence on the regulator is gone, but dependence upon the cutoff remains. Let us examine the NR and ER limits

$$(2F^{(1)}(q^2) + \delta_{\text{infr}})_{\text{IR}} = \frac{\alpha}{\pi}\frac{q^2}{3m^2}\log\frac{m^2}{-q^2} \quad \text{(NR)}, \tag{52}$$

$$(2F^{(1)}(q^2) + \delta_{\text{infr}})_{\text{IR}} = -\frac{\alpha}{\pi}\log\frac{-q^2}{m^2}\log\frac{-q^2}{4\Lambda^2} \quad \text{(ER)}. \tag{53}$$

The extreme relativistic calculation highlights another issue: if the cutoff photon energy Λ separating 'infrared' from 'hard' photons is chosen to be sufficiently small, then the overall scattering cross section can become negative. This is obviously absurd and can be rectified by considering *multiple* infrared photon emissions whose overall momenta totals to Λ [42, 48].

ORCID iDs

David C Latimer https://orcid.org/0000-0002-6904-2191

References

[1] Larmor J 1897 LXIII. On the theory of the magnetic influence on spectra; and on the radiation from moving ions *Phil. Mag.* **44** 503–12
[2] Lorentz H A 1904 Weiterbildung der maxwellschen theorie v 2 *Enzyklopädie der Mathematischen Wissenschaften* ed A Sommerfeld (Leipzig: Teubner) pp 145–288
[3] Abraham M 1905 *Theorie der Elektrizität Vol. II. Elektromagnetische Strahlung* (Leipzig: Teubner)
[4] Dirac P A M 1938 Classical theory of radiating electrons *Proc. R. Soc.* A **167** 148–69
[5] Rohrlich F 1965 *Classical Charged Fields* (Reading: Addison-Wesley)
[6] David J Griffiths 2013 *Introduction to Electrodynamics* 4th edn (Boston, MA: Pearson) pp 491–2
[7] Eliezer C J 1943 The hydrogen atom and the classical theory of radiation *Math. Proc. Camb. Phil. Soc.* **39** 173–80
[8] Kasher J C 1976 One-dimensional central-force problem, including radiation reaction *Phys. Rev.* D **14** 939–44
[9] Plass G N 1961 Classical electrodynamic equations of motion with radiative reaction *Rev. Mod. Phys.* **33** 37–62
[10] Huschilt J and Baylis W E 1976 Numerical solutions to two-body problems in classical electrodynamics: head-on collisions with retarded fields and radiation reaction: I. Repulsive case *Phys. Rev.* D **13** 3256–61
[11] Baylis W E and Huschilt J 1976 Numerical solutions to two-body problems in classical electrodynamics: head-on collisions with retarded fields and radiation reaction: II. Attractive case *Phys. Rev.* D **13** 3262–8
[12] Comay E 1991 Stability problems of numerical solutions to the Lorentz–Dirac equation *Appl. Math. Lett.* **4** 11–4
[13] Huschilt J and Baylis W E 1978 Rutherford scattering with radiation reaction *Phys. Rev.* D **17** 985–93
[14] Comay E 1996 Solutions of the Lorentz–Dirac equation in the ultrarelativistic domain *J. Phys. A: Math. Gen.* **29** 2111
[15] Landau L D and Lifshitz E M 1980 *The Classical Theory of Fields* 4th edn (Oxford: Butterworth-Heinemann)
[16] Griffiths D J, Proctor T C and Schroeter D F 2010 Abraham–Lorentz versus Landau–Lifshitz *Am. J. Phys.* **78** 391–402
[17] Levine H, Moniz E J and Sharp D H 1977 Motion of extended charges in classical electrodynamics *Am. J. Phys.* **45** 75–8
[18] Yaghjian A 2006 *Relativistic Dynamics of a Charged Sphere* 2nd edn (New York: Springer)
[19] Rohrlich F 1999 Classical self-force *Phys. Rev.* D **60** 084017
[20] Rohrlich F 2008 Dynamics of a charged particle *Phys. Rev.* E **77** 046609
[21] Parrott S 2002 Asymptotics of Rohrlich's equation of motion for charged particles arXiv:gr-qc/0205065 [gr-qc]
[22] Parrott S 2005 Comment on Phys. Rev. D 60 084017 'classical self-force' by F Rohrlich arXiv:gr-qc/0502029 [gr-qc]

[23] Moniz E J and Sharp D H 1974 Absence of runaways and divergent self-mass in nonrelativistic quantum electrodynamics *Phys. Rev.* D **10** 1133–6
[24] Moniz E J and Sharp D H 1977 Radiation reaction in nonrelativistic quantum electrodynamics *Phys. Rev.* D **15** 2850
[25] Sharp D H 1980 Radiation reaction in nonrelativistic quantum theory *Foundations of Radiation Theory and Quantum Electrodynamics* ed A O Barut (New York: Springer) pp 127–41
[26] Higuchi A 2002 Radiation reaction in quantum field theory *Phys. Rev.* D **66** 105004
Higuchi A 2004 *Phys. Rev.* D **69** 129903 erratum
[27] Higuchi A and Martin G D R 2004 Lorentz–Dirac force from qed for linear acceleration *Phys. Rev.* D **70** 081701
[28] Higuchi A and Martin G D R 2005 Classical and quantum radiation reaction for linear acceleration *Found. Phys.* **35** 1149–79
[29] Higuchi A and Martin G D R 2006 Radiation reaction on charged particles in three-dimensional motion in classical and quantum electrodynamics *Phys. Rev.* D **73** 025019
[30] Higuchi A and Martin G D R 2006 Quantum radiation reaction and the green's function decomposition *Phys. Rev.* D **74** 125002
[31] Krivitsky V S and Tsytovich V N 1991 Average radiation reaction force in quantum electrodynamics *Sov. Phys. Usp.* **34** 250–8
Krivitsky V S and Tsytovich V N 1991 *Usp. Fiz. Nauk* **161** 125
[32] Ilderton A and Torgrimsson G 2013 Radiation reaction in strong field qed *Phys. Lett.* B **725** 481–6
[33] Jauch J M and Rohrlich F 1976 *The Theory of Photons and Electrons* (Berlin: Springer)
[34] Hindmarsh A C 1983 ODEPACK, a systematized collection of ODE solvers *Scientific Computing* (*IMACS Transactions on Scientific Computation* vol 1) ed R S Stepleman *et al* (Amsterdam: North-Holland) pp 55–64
[35] Radhakrishnan K and Hindmarsh A C 1993 Description and use of LSODE, the Livermore solver for ordinary differential equations *LLNL Report* UCRL-ID-113855 Lawrence Livermore National Laboratory
[36] Brown P N and Hindmarsh A C 1989 Reduced storage matrix methods in stiff ODE systems *Appl. Math. Comput.* **31** 40–91 Special Issue Numerical Ordinary Diferrential equations (Proc. of the 1986 ODE Conf.)
[37] Gupta S N 1955 Multiple bremsstrahlung *Phys. Rev.* **99** 1015–9
[38] Mahanthappa K T 1962 Multiple production of photons in quantum electrodynamics *Phys. Rev.* **126** 329–40
[39] Rajeev S G 2008 Exact solution of the Landau–Lifshitz equations for a radiating charged particle in the Coulomb potential *Ann. Phys.* **323** 2654–61
[40] Dalitz R H 1951 On higher born approximations in potential scattering *Proc. R. Soc.* A **206** 509–20
[41] Holstein B R 2007 Second born approximation and coulomb scattering *Am. J. Phys.* **75** 537–9
[42] Yennie D R, Frautschi S C and Suura H 1961 The infrared divergence phenomena and high-energy processes *Ann. Phys.* **13** 379–452
[43] Bethe H and Heitler W 1934 On the stopping of fast particles and on the creation of positive electrons *Proc. R. Soc.* A **146** 83–112
[44] Furry W H 1951 On bound states and scattering in positron theory *Phys. Rev.* **81** 115–24
[45] Rohrlich F 1950 Quantum electrodynamics of charged particles without spin *Phys. Rev.* **80** 666–87
[46] Vermaseren J A M 2000 New features of FORM arXiv:math-ph/0010025
[47] 't Hooft G and Veltman M J G 1979 Scalar one loop integrals *Nucl. Phys.* B **153** 365–401
[48] Peskin M E and Schroeder D V 1995 *An Introduction to Quantum Field Theory* (Reading: Addison-Wesley)
[49] Eriksson B L K E and Rinander G A 1963 Radiative corrections to muon-electron scattering *Nuovo Cim.* **30** 1434
[50] Eriksson K E 1961 Radiative corrections to muon-electron scattering *Nuovo Cim.* **19** 1029
[51] Passarino G and Veltman M J G 1979 One loop corrections for $e^+ e^-$ annihilation into $\mu^+ \mu^-$ in the Weinberg model *Nucl. Phys.* B **160** 151–207
[52] Eriksson K E 1961 On radiative corrections due to soft photons *Nuovo Cim.* **19** 1010–28